

Discontinuous Shear Thickening of Frictional Hard-Sphere Suspensions

Ryohei Seto,¹ Romain Mari,¹ Jeffrey F. Morris,^{1,2} and Morton M. Denn^{1,2}

¹*Benjamin Levich Institute, City College of New York, New York, NY 10031, USA*

²*Department of Chemical Engineering, City College of New York, New York, NY 10031, USA*

(Dated: October 8, 2013)

Discontinuous shear thickening (DST) observed in many dense athermal suspensions has proven difficult to understand and to reproduce by numerical simulation. By introducing a numerical scheme including both relevant hydrodynamic interactions and granularlike contacts, we show that contact friction is essential for having DST. Above a critical volume fraction, we observe the existence of two states: a low viscosity, contactless (hence, frictionless) state, and a high viscosity frictional shear jammed state. These two states are separated by a critical shear stress, associated with a critical shear rate where DST occurs. The shear jammed state is reminiscent of the jamming phase of granular matter. Continuous shear thickening is seen as a lower volume fraction vestige of the jamming transition.

Suspensions of particles at high volume fraction of solid, often termed dense suspensions, have a rich non-Newtonian rheology. This is particularly striking for the simple system of nearly rigid particles in a Newtonian fluid, which exhibits shear thinning, shear thickening, and normal stresses, the last associated with strong microstructural distortion, despite the dominant influence played in such mixtures by viscous (Stokes-flow) fluid mechanics [1]. The phenomenon of discontinuous shear thickening (DST) (see [2–5] and references therein) is especially fascinating. Suspensions exhibiting DST flow relatively easily with slow stirring, but become highly viscous or even seemingly solid if one tries to stir them rapidly. In a rheometer, the transition is seen at a critical shear rate for a given volume fraction. It is often found that DST is completely reversible [6]. DST typically occurs for a volume fraction that exceeds a threshold value ϕ_c , which depends on the nature of the suspended particles: increased nonsphericity or surface roughness seem to lower ϕ_c . Continuous shear thickening (CST) is observed below ϕ_c , and becomes weaker with decreasing volume fraction. Although counterintuitive, the abrupt or discontinuous increase of viscosity with increase of shear rate is a generic feature of dense suspensions [3, 7], occurring in both Brownian (colloidal) and non-Brownian suspensions. This ubiquity suggests the possibility of a single mechanistic basis applicable to the various types of suspension. DST has yet to be reproduced by a simulation method which can unambiguously point to the essential physical features necessary for its observation. This Letter presents a novel method able to identify these features.

Several possible mechanisms have been proposed as the origin of DST. An order-disorder mechanism [8–10] describes a low shear rate ordered flow with few interactions between particles that becomes unstable at high shear rates and evolves to a disordered, highly interacting viscous flow. A hydroclustering [6, 11–15] or (hydro)contact network [16, 17] mechanism attributes the thickening to clusters of particles “glued” together by the lubrication

singularity. The competition between a force (Brownian or interparticle) tending to keep particles apart and the imposed shear strain, which tends to push particles together along the compressional axis, results in narrower interparticle gaps as the shear rate increases. The resulting clusters of particles move more rigidly, effectively increasing the viscosity. Neither of these scenarios makes a distinction between CST and DST, and the development of hydroclusters oriented with their dominant principal axis in the compressional quadrant in Brownian hard-sphere suspensions leads only to CST [18, 19] even at volume fractions as large as $\phi = 0.58$ [20]. A theoretical approach based on an *ad hoc* mode-coupling theory attempts to describe DST as a shear-induced glass transition [21–24]. Another suggested mechanism [5, 25–27] explicitly relates DST to the existence of an underlying jamming transition due to the frustration of the granularlike dilatancy by the confining stress.

The appropriate mechanism has been difficult to ascertain. Most of the mechanisms noted predict the shear rate above which shear thickening happens [5, 28, 29]. Experimentally, the order-disorder transition seems unnecessary [30], at least with a strictly ordered state [10]. Simulations based on purely hydrodynamic modeling, such as Stokesian Dynamics [12], show that hydroclusters appear in the semidilute regime and networks in the concentrated regime ($\phi \gtrsim 0.5$), where they produce a (weak) CST [13, 16, 31, 32]. DST has never been reproduced by those models.

A key mechanical issue left largely unconsidered in previous simulation efforts is the occurrence of contacts, and, in particular, frictional contacts between particles. It is known that, despite the lubrication force, particle roughness can lead to contacts, resulting in qualitative changes from the expected behavior of ideal smooth hard particles [33, 34]. One consequence of surface contact is an increase of viscosity with increasing surface friction [35]. In a colloidal silica suspension exhibiting DST, increased particle roughness has been shown to lead to a smaller critical shear rate [36, 37]. Even for ideally

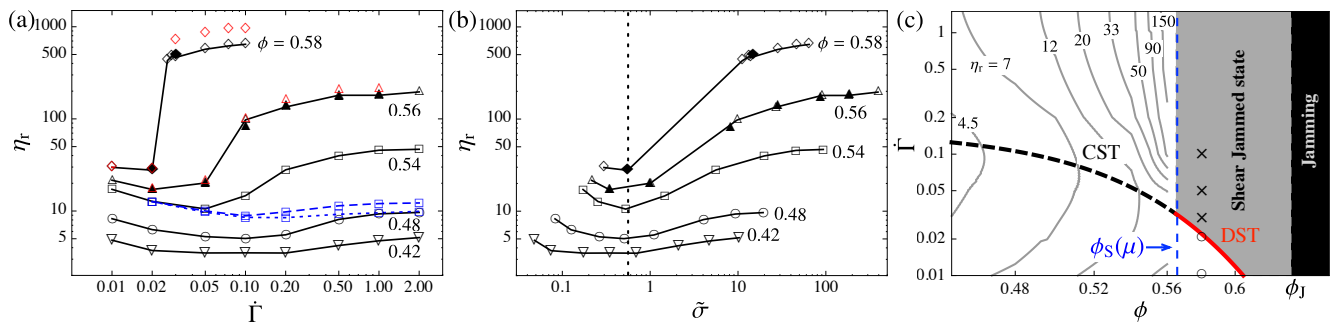


FIG. 1. (color online) (a), (b) Shear rate and stress dependence of the relative viscosity η_r , respectively. $\dot{\Gamma}$ is the dimensionless shear rate. The open and filled symbols indicate the results of $n = 512$ and 2048 , and the volume fractions are shown in the graphs. The friction coefficient is $\mu = 1$ except for the dashed and dotted blue lines, for which $\mu = 0.1$ and 0 , respectively. Red symbols show the results with 1.5 times stiffer particles. (c) DST (red line) and CST (dashed line) are shown in the phase diagram. The former is expected to reach the jamming point ϕ_J for $\dot{\Gamma} \rightarrow 0$, which is not seen because of log scale. The contour lines for $\phi < 0.56$ are labeled by the relative viscosity, $\eta_r(\phi, \dot{\Gamma})$. Before jamming (black domain), the shear jammed states (gray domain) exist. Observed flowing and jammed states at $\phi = 0.58$ are shown by circles and crosses, respectively.

smooth spheres, such issues as finite particle deformability may play a role for the large stresses that arise at small interparticle gaps. Such small gaps, dropping to subnanometer scale even for noncolloidal particles, lead us to question the relevant physics of close particle interactions. The experiments cited above, as well as physical intuition, suggest that contact between particles is an essential ingredient of the mechanics of flow of highly concentrated suspensions.

In this Letter we introduce a numerical model merging hydrodynamics and features of granular physics. The model permits contacts between particles by assuming a cutoff in the singular resistance due to lubrication for a small interparticle gap in the Stokes regime. These contacts are treated with a model adopted from granular physics, involving friction. Our simulations, limited here to athermal systems (i.e., not considering Brownian motion, although this may, in principle, be introduced), show expected effects of volume fraction and exhibit both CST and DST, with the critical ingredient leading to the latter being the incorporation of interparticle friction (FIG. 1).

Our model deals with the following interparticle interactions: the hydrodynamic force \mathbf{F}_H , the contact force \mathbf{F}_C , and a repulsive force \mathbf{F}_R . Since both fluid and particle inertia are neglected, the dynamics is overdamped and forces (and torques) are balanced for each particle: $\mathbf{F}_H^{(i)} + \mathbf{F}_C^{(i)} + \mathbf{F}_R^{(i)} = 0$, $i = 1, \dots, N$. The hydrodynamic interaction \mathbf{F}_H in the Stokes regime can be written as a linear function of velocities of particles \mathbf{U} relative to an imposed flow \mathbf{U}^∞ by constructing a resistance matrix \mathbf{R} ; i.e., hydrodynamic forces are of the form $\mathbf{F}_H = -\mathbf{R} \cdot (\mathbf{U} - \mathbf{U}^\infty)$ (see [12, 38] for details). The particle velocities can therefore be determined by solving the force balance equations.

For concentrated suspensions, the resistance matrix

can be approximately obtained by neglecting the far-field or many-body effects and taking the leading terms of the pair hydrodynamic interactions [38]. In the simulations, we use the leading terms from the exact solution for two particles [39, 40] in order to handle bidisperse systems, but the following explanation assumes a monodisperse system for simplicity. There is a singular factor $1/h^{(i,j)}$ in the resistance to relative motion of particles i and j , where $h^{(i,j)}$ is the interparticle gap. We argue that it is appropriate, in seeking to represent real suspensions, to relax the idealization to represent factors such as the finite roughness of particle surfaces. We regularize the lubrication by inserting a small length δ to prevent divergence at contact $h^{(i,j)} = 0$ as in [41] ($\delta = 10^{-3}a$ is used, where a is the particle radius). The squeezing mode of the lubrication force is written as

$$\mathbf{F}_{\text{lub}}^{(i,j)} = -\alpha(h^{(i,j)}) (\mathbf{U}^{(i)} - \mathbf{U}^{(j)}) \cdot \mathbf{n}^{(i,j)} \mathbf{n}^{(i,j)}. \quad (1)$$

Here $\alpha(h) = 3\pi\eta_0 a^2 / 2(h + \delta)$, where η_0 is the viscosity of the suspending fluid. $\mathbf{n}^{(i,j)}$ is the unit vector along the line of centers from particle i to j . Thus, the hydrodynamic force acting on a particle is approximately given as the sum of the regularized lubrication force and the Stokes drag $\mathbf{F}_{\text{Stokes}}^{(i)} = -6\pi\eta_0 a \{\mathbf{U}^{(i)} - \mathbf{U}^\infty(\mathbf{r}^{(i)})\}$. The hydrodynamic forces scale with shear rate $\dot{\gamma}$, and hence there is no essential shear-rate dependence.

The contact force \mathbf{F}_C is activated for $h^{(i,j)} < 0$. A simple spring-and-dashpot contact model [41–43] is employed to mimic frictional hard spheres; the normal force is proportional to the overlap $-h^{(i,j)}$: $\mathbf{F}_{C,\text{nor}}^{(i,j)} = k_n h^{(i,j)} \mathbf{n}^{(i,j)}$, where k_n is the spring constant. The friction appears as a tangential force and a torque, both proportional to the tangential spring displacement $\boldsymbol{\xi}^{(i,j)}$: $\mathbf{F}_{C,\text{tan}}^{(i,j)} = k_t \boldsymbol{\xi}^{(i,j)}$ and $\mathbf{T}_C^{(i,j)} = k_t a \mathbf{n}^{(i,j)} \times \boldsymbol{\xi}^{(i,j)}$ (see [43] for details), where k_t is the tangential spring constant. The tangential force is subject to Coulomb's law

$\mathbf{F}_{C,\text{tan}} < \mu \mathbf{F}_{C,\text{nor}}$. Even with contact forces, ideal hard-sphere suspensions should be Newtonian, because different $\dot{\gamma}$ result in the same particle trajectories, but with different time ($\sim 1/\dot{\gamma}$) and force ($\sim \dot{\gamma}$) scales. When trying to mimic hard spheres with linear springs, we should avoid introducing an artificial shear-rate dependence. We therefore choose k_n and $k_t \sim \dot{\gamma}$, and tune the dashpot resistance to keep a short contact relaxation time ($= 10^{-3}/\dot{\gamma}$), in contrast to [16].

The shear-rate dependence is introduced by another force that is not scaled with $\dot{\gamma}$, which we take as an electrostatic double-layer force [44]. The approximate form $\mathbf{F}_R^{(i,j)} = -Ca e^{-\kappa h^{(i,j)}} \mathbf{n}^{(i,j)}$ is used for $h^{(i,j)} > 0$, with $1/\kappa = 0.05a$. The repulsive force acts to keep particle gaps wider, and is more effective at small shear rate, i.e., where the shear time $1/\dot{\gamma}$ is longer. We thus introduce a dimensionless shear rate as a ratio of two force scales: $\dot{\Gamma} \equiv 6\pi\eta_0 a^2 \dot{\gamma} / |\mathbf{F}_R(h=0)|$, which is analogous to the Péclet number for Brownian suspensions.

Simulations are performed using Lees-Edwards boundary conditions. The simulation boxes are cubes for $n = 512$ particles and rectangular parallelepipeds (the shear plane is square, and the depth is one half of the other dimensions) for $n = 2048$. The influence of particle migration, as previously discussed [45], can be ruled out here since the system is homogeneous owing to the boundary conditions. A bidisperse system is investigated to avoid strong ordering ($a_2 = 1.4a_1$ and $\phi_1 \approx \phi/2$, i.e., $n_1/n \approx 0.73$), thereby reducing the potential for an order-disorder transition [8–10].

We obtain the dependence of the relative viscosity η_r on the dimensionless shear rate $\dot{\Gamma}$ and stress $\bar{\sigma}$ ($\equiv \eta_r \dot{\Gamma}$) for a range of volume fractions ϕ and friction coefficients μ , as shown in FIG. 1. Two major conclusions can be drawn. The first is that for frictional spheres, a transition from CST to DST is observed upon increase of ϕ . For $\mu = 1$, the transition occurs at $0.56 < \phi_c < 0.58$. Although the shear rate at the onset of thickening decreases with increasing ϕ , the onset stress σ_{on} is constant, as shown in FIG. 1(b). This is consistent with experimental observations [28, 29]. For $\phi > \phi_c$, the high viscosity state achieved at high shear rate is strongly dependent on the particle stiffness, while no such dependence is seen for $\phi < \phi_c$ or in the low viscosity state. Remarkably, this qualitative difference between CST and DST has been observed in experiments [5, 25, 27]. There, the control parameter is confinement, not particle stiffness, but both play the key role for the system to overcome the jammed state: in experiments by dilation, in simulations by particle overlap. This has an important conceptual consequence: if one considers a suspension of ideal hard frictional spheres sheared at fixed volume, the system becomes solid above the critical shear stress σ_{on} , as the jammed state achieved is stable against any further increment of shear stress.

The second basic result is the crucial importance of

friction. For $\mu = 0.1$, the thickening is substantially weaker than for $\mu = 1$, and it is completely absent in the frictionless case, even at volume fractions approaching the jamming point ϕ_J . This means that friction is essential for a shear jammed state to exist. A similar finding is reported for dry granular materials [46, 47].

One is then led to think that shear thickening is related to a shear-induced jamming, similar to what was suggested in [25, 26, 48]. To test this idea, we show in FIG. 2(a) the spatial distribution of contact bonds in the system, in both the low and high viscosity phases. The difference is striking: for low shear rate, contact force chains appear, but only as elongated and isolated objects (unique to the combined hydrodynamic-plus-contact force algorithm) along the compression axis, whereas for high shear rate, a network percolates in all directions. Similar observations have been made for shear jammed states in granular materials [46].

Cates *et al.* [48] proposed a simple model of shear jammed states, describing them by a stress tensor $\boldsymbol{\sigma} = \Lambda_1 \mathbf{nn} + \Lambda_2 \mathbf{mm} + \Lambda_3 \mathbf{ll}$, where \mathbf{n} , \mathbf{m} , and \mathbf{l} are the three principal axes of the system, corresponding to the three preferential orientations of force chains. In our simulations, within a one or two degree accuracy, they coincide with the compression (\mathbf{n}), vorticity (\mathbf{m}), and elongation (\mathbf{l}) axes for all conditions investigated.

We show that the minimal model can capture most of the physics of shear thickening, provided that one distinguishes between the total stress $\boldsymbol{\sigma}$ and the contribution from frictional contact forces $\boldsymbol{\sigma}^c$. The associated eigenvalues Λ_i and Λ_i^c normalized by their traces are shown in FIG. 2(b). It is clear that the result for the total stress shows no difference between low and high viscosity states; the multiaxial stress structure is observed in both states, meaning that, at such high volume fractions, the total force chains are percolating in all directions. However, the shear thickening coincides with a dramatic change in the contact stress. At low shear rate, contacts along the compression axis dominate the stress, whereas the load is also shared by the other two axes at high shear rate. The role of friction can be seen by examining the eigenvalues Λ_i^c in the frictionless contact case, as shown in FIG. 2(b): even though the contact stress also gradually evolves from a uniaxial to a multiaxial form, no shear thickening is observed. In addition, the largest contact clusters for frictional and frictionless cases are compared in FIG. 2(c). Clearly, friction advances the percolation; frictional contacts under shear cause local dilatancy, which compresses remaining gaps. Thus, friction is essential for the multiaxial contact network to develop sharply, i.e., over a narrow range of shear rate, and to display the observed mechanical properties.

The percolation of the contact network occurs for a minimum shear stress σ_{on} , which is apparently the point where repulsive forces among particles are not sufficient to prevent the proliferation of contacts.

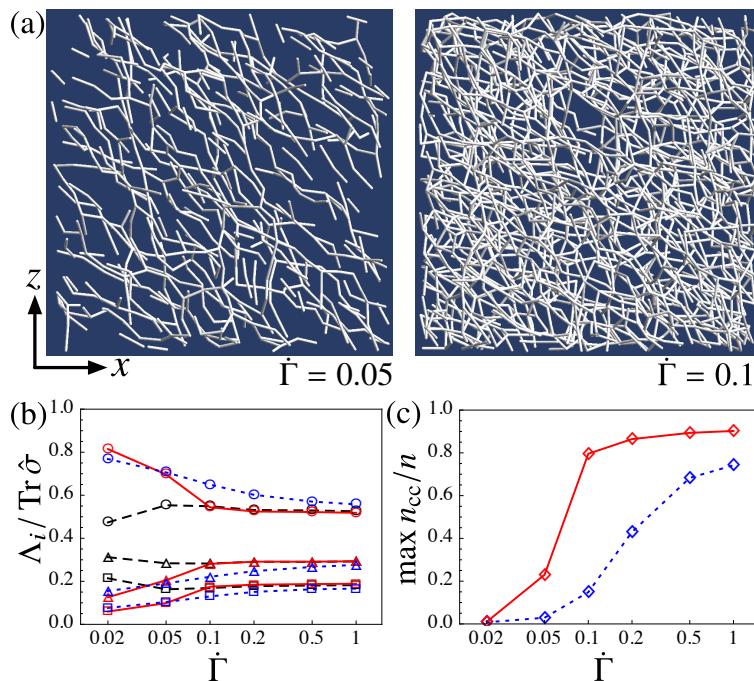


FIG. 2. (a) Particle contacts are visualized as bonds at the two shear rates $\dot{\Gamma} = 0.05$ and $\dot{\Gamma} = 0.1$ exhibiting low and high viscosity states, respectively ($\mu = 1$, $\phi = 0.56$, $n = 2048$). (b) The stress eigenvalues, Λ_1 (circles), Λ_2 (triangles), and Λ_3 (squares), normalized by the trace, are shown ($\phi = 0.56$, $n = 512$). The solid lines (red) indicate the contact stress σ^c , and dashed lines (black) the total stress σ ($\mu = 1$). The dotted lines (blue) show the contact stress of the frictionless system ($\mu = 0$). (c) The largest contact clusters for $\mu = 1$ (solid red) and $\mu = 0$ (dotted blue) are compared, where n_{cc} is number of particles in a cluster.

DST is observed when the percolating network can elastically sustain an applied stress. This is only possible for a minimum volume fraction $\phi > \phi_c$, where there are enough constraints to “lock” or “jam” the structure. The critical volume fraction can be identified as the shear jamming [46]: $\phi_c = \phi_S(\mu)$. It is close to the values observed for the static jamming of frictional spheres, but it need not be the same [46]. When the suspension is forced to flow at high shear rate in a strain-controlled experiment, the viscosity is dominated by the yield stress of the solid network, which is itself influenced by the confinement. The network of contacts is constantly broken and reformed, going from one transient solid configuration to another.

For $\phi < \phi_S(\mu)$, the CST is a vestige of this jamming transition. Even when the applied shear stress is larger than σ_{on} , no strictly jammed contact network can form. Only underconstrained structures appear for $\sigma > \sigma_{on}$ (or equivalently $\dot{\Gamma} > \dot{\Gamma}_c$), reminiscent of the jammed states seen for $\phi > \phi_S(\mu)$. These structures still require a large applied stress to flow, as they are only deformable via collective rearrangements. Upon decrease of ϕ , these networks are increasingly underconstrained, and the high viscosity phase fades away. It is worth noticing that the low viscosity phase, essentially frictionless (as there are fewer frictional contacts), has similar behavior, form-

ing force networks increasingly constrained as the volume fraction increases [49, 50]. It is indeed seen in FIG. 1 (a) that the viscosity also increases with ϕ in this phase. However, the point where solid frictionless structures appear is only reached for $\phi = \phi_J$, which is much larger than $\phi_S(\mu)$. The fact that these two divergences occur at two different volume fractions is the cause for the blowup of the difference of viscosity between the low shear rate frictionless state and the high shear rate frictional state as $\phi \rightarrow \phi_S(\mu)$.

The above results lead us to propose a schematic phase diagram for the shear thickening of athermal suspensions, represented in the ϕ - $\dot{\Gamma}$ plane in FIG. 1 (c). DST, denoted by a solid (red) line, occurs in the range $\phi_S(\mu) < \phi < \phi_J$ for a critical shear stress σ_{on} . Asymptotically, in the low viscosity frictionless phase, $\eta \propto (1 - \phi/\phi_J)^{-q}$ with $q = 2$ [49], which gives for the critical shear rate $\dot{\Gamma}_c \propto \sigma_{on} (1 - \phi/\phi_J)^2$. This scaling is, however, difficult to observe in our data range, as we are still rather far from the divergence. Above the red line, the shear stress is a yield stress of the shear jammed state, proportional to the pressure. For ideal hard spheres sheared at constant volume, this region would simply be inaccessible, as the yield stress would be infinite. Below $\phi_S(\mu)$, CST occurs around an isostress dashed black line, which appears as the continuation of the DST red line. The stress is domi-

nated by the proximity of shear jammed states above this dashed line, and gives a viscosity $\eta \propto (1 - \phi/\phi_S(\mu))^{-q'}$ with an estimated $q' \approx 1.5$.

This phase diagram may well be valid even in the case of Brownian suspensions, where Brownian motion may play a role similar to the double-layer force, namely preventing contacts and reopening gaps at low shear rate.

We thank Ehssan Nazockdast for very useful and stimulating discussions. J.F.M. was supported in part by NSF PREM (DMR 0934206).

-
- [1] J. F. Morris, *Rheol Acta* **48**, 909 (2009).
- [2] A. B. Metzner and M. Whitlock, *Trans. Soc. Rheol.* **2**, 239 (1958).
- [3] H. A. Barnes, *J. Rheol.* **33**, 329 (1989).
- [4] J. Mewis and N. J. Wagner, *Colloidal Suspension Rheology* (Cambridge University Press, Cambridge, England, 2011).
- [5] E. Brown and H. M. Jaeger, *J. Rheol.* **56**, 875 (2012).
- [6] J. Bender and N. J. Wagner, *J. Rheol.* **40**, 899 (1996).
- [7] E. Brown, N. A. Forman, C. S. Orellana, Z. Hanjun, B. W. Maynor, D. E. Betts, J. M. DeSimone, and H. M. Jaeger, *Nature Mater.* **9**, 220 (2010).
- [8] R. L. Hoffman, *Trans. Soc. Rheol.* **16**, 155 (1972).
- [9] R. L. Hoffman, *J. Colloid Interface Sci.* **46**, 491 (1974).
- [10] R. L. Hoffman, *J. Rheol.* **42**, 111 (1998).
- [11] J. F. Brady and G. Bossis, *J. Fluid Mech.* **155**, 105 (1985).
- [12] J. F. Brady and G. Bossis, *Annu. Rev. Fluid Mech.* **20**, 111 (1988).
- [13] G. Bossis and J. F. Brady, *J. Chem. Phys.* **91**, 1866 (1989).
- [14] J. W. Bender and N. J. Wagner, *J. Colloid Interface Sci.* **172**, 171 (1995).
- [15] N. J. Wagner and J. F. Brady, *Phys. Today* **62**, 27 (2009).
- [16] J. R. Melrose and R. C. Ball, *J. Rheol.* **48**, 937 (2004).
- [17] J. R. Melrose and R. C. Ball, *J. Rheol.* **48**, 961 (2004).
- [18] D. R. Foss and J. F. Brady, *J. Fluid Mech.* **407**, 167 (2000).
- [19] E. Nazockdast and J. F. Morris, *J. Fluid Mech.* **713**, 420 (2012).
- [20] J. F. Morris and B. Katyal, *Phys. Fluids* **14**, 1920 (2002).
- [21] C. B. Holmes, M. Fuchs, and M. E. Cates, *Europhys. Lett.* **63**, 240 (2003).
- [22] C. B. Holmes, M. E. Cates, M. Fuchs, and P. Sollich, *J. Rheol.* **49**, 237 (2005).
- [23] M. E. Cates, M. D. Haw, and C. B. Holmes, *J. Phys.: Condens. Matter* **17**, S2517 (2005).
- [24] M. Sellitto and J. Kurchan, *Phys. Rev. Lett.* **95**, 236001 (2005).
- [25] A. Fall, N. Huang, F. Bertrand, G. Ovarlez, and D. Bonn, *Phys. Rev. Lett.* **100**, 018301 (2008).
- [26] E. Brown and H. M. Jaeger, *Phys. Rev. Lett.* **103**, 086001 (2009).
- [27] A. Fall, F. Bertrand, G. Ovarlez, and D. Bonn, *J. Rheol.* **56**, 575 (2012).
- [28] W. H. Boersma, J. Laven, and H. N. Stein, *AIChE J.* **36**, 321 (1990).
- [29] B. J. Maranzano and N. J. Wagner, *J. Chem. Phys.* **114**, 10514 (2001).
- [30] B. J. Maranzano and N. J. Wagner, *J. Chem. Phys.* **117**, 10291 (2002).
- [31] T. N. Phung, J. F. Brady, and G. Bossis, *J. Fluid Mech.* **313**, 181 (1996).
- [32] A. Sierou and J. F. Brady, *J. Rheol.* **46**, 1031 (2002).
- [33] P. A. Arp and S. G. Mason, *J. Colloid Interface Sci.* **61**, 44 (1977).
- [34] Y. Zhao and R. H. Davis, *Chem. Eng. Sci.* **57**, 1997 (2002).
- [35] J. Castle, A. Farid, and L. V. Woodcock, *Prog. Colloid Polym. Sci.* **100**, 259 (1996).
- [36] D. Lootens, P. Hébraud, E. Lécolier, and H. Van Damme, *Oil Gas Sci. Technol.* **59**, 31 (2004).
- [37] D. Lootens, H. van Damme, Y. Hémar, and P. Hébraud, *Phys. Rev. Lett.* **95**, 268302 (2005).
- [38] R. C. Ball and J. R. Melrose, *Physica A* **247**, 444 (1997).
- [39] D. J. Jeffrey and Y. Onishi, *J. Fluid Mech.* **139**, 261 (1984).
- [40] D. J. Jeffrey, *Phys. Fluids A* **4**, 16 (1992).
- [41] M. Trulsson, B. Andreotti, and P. Claudin, *Phys. Rev. Lett.* **109**, 118305 (2012).
- [42] P. A. Cundall and O. D. L. Strack, *Geotechnique* **29**, 47 (1979).
- [43] S. Luding, *Granular Matter* **10**, 235 (2008).
- [44] J. N. Israelachvili, *Intermolecular and surface forces* (Academic Press, 2011).
- [45] A. Fall, A. Lemaître, F. Bertrand, D. Bonn, and G. Ovarlez, *Phys. Rev. Lett.* **105**, 268303 (2010).
- [46] D. Bi, J. Zhang, B. Chakraborty, and R. P. Behringer, *Nature* **480**, 355 (2011).
- [47] M. Otsuki and H. Hayakawa, *Phys. Rev. E* **83**, 051301 (2011).
- [48] M. E. Cates, J. P. Wittmer, J.-P. Bouchaud, and P. Claudin, *Phys. Rev. Lett.* **81**, 1841 (1998).
- [49] E. Lerner, G. Düring, and M. Wyart, *Proc. Natl. Acad. Sci. USA* **109**, 4798 (2012).
- [50] E. Lerner, G. Düring, and M. Wyart, *Europhys. Lett.* **99**, 58003 (2012).